

# Nonlinear Panel Flutter Using High-Order Triangular Finite Elements

A.D. Han\* and T.Y. Yang†  
*Purdue University, West Lafayette, Indiana*

A 54 degree-of-freedom, high-order triangular plate finite element extended for geometrically nonlinear static and dynamic analysis is used to formulate and analyze the supersonic nonlinear panel flutter problems. The finite element formulation is based on Kirchhoff's theory of thin plates. The quasisteady aerodynamic theory is used. Numerical solution procedures are presented. The limit cycle oscillation analyses are performed for two-dimensional and square panels with all edges simply supported and clamped, respectively. The effects of in-plane compressive force, mass ratio, and in-plane edge stress free condition are considered. Stress distributions for the limit cycle oscillation of a two-dimensional panel are plotted. For the case of panels under static pressure differential, the results for the steady mean amplitude and flutter dynamic pressure are obtained for the two-dimensional and square panels, respectively. The effect of biaxial in-plane compressive stress for a simply supported square panel is studied and boundaries among the flat and stable region, dynamically stable buckled region, and the limit cycle oscillation region are found. Alternative analytical and numerical solutions are available for most of the examples for comparison and all are in excellent agreement.

## Introduction

FLUTTER of a panel in the supersonic flow falls in the category of self-excited oscillations. Panel flutter differs from wing flutter in that the aerodynamic force acts only on one side of the panel and that the phenomenon of the panel flutter is generally less catastrophic than wing flutter. Small amplitude linear structural theory indicates that there is a critical dynamic pressure above which the panel motion becomes unstable and grows exponentially with time. In reality, however, geometrically nonlinear effect is present due to vibration with large amplitudes. The panel not only bends but also stretches with in-plane tensile stresses. Such in-plane tensile stresses provide a stabilizing effect which restrains the panel motion to bound limit cycle oscillations with increasing amplitude as the dynamic pressure increases. The skin panels of the flight vehicle can thus withstand velocities beyond those predicted based on the small amplitude linear structural theory. For a more thorough understanding and more realistic assessment of the panel flutter problems, the geometrically nonlinear effect due to large amplitude oscillations should be considered. An outstanding survey of the studies on both the linear and nonlinear panel flutter was given by Dowell<sup>1</sup> in 1970. The basic theories and a detailed account of the developments on panel flutter can be found in Ref. 2.

Various analytical methods exist for the investigation of the problems of nonlinear panel flutter in supersonic flow. Generally, Galerkin's method can be used in the space domain and techniques, such as direct time integration method,<sup>3-5</sup> harmonic balance method,<sup>6-9</sup> and perturbation method<sup>9-11</sup> can be used in the time domain to determine the properties of the limit cycle oscillation. Eastep and McIntosh<sup>8</sup> used the Rayleigh-Ritz approximation to Hamilton's variational principle instead of Galerkin's method to set up the equations of motion in the space domain.

Applications of the finite element method to the linear panel flutter problems have been studied by many investigators.<sup>12-23</sup> A review of the applications of the finite

element displacement method to the linear panel flutter problems was given by Yang and Sung.<sup>23</sup> Yang and Han<sup>24</sup> extended the finite element formulation given by Olson<sup>12</sup> to study the flutter boundaries for the two-dimensional panels buckled due to an in-plane force caused by aerodynamic heating.

Mei and Rogers<sup>25</sup> modified the NASTRAN code (level 16.0) to analyze the supersonic flutter problem of two-dimensional panels oscillating with large amplitudes. Mei<sup>26</sup> later applied the finite element displacement approach to study the limit cycle oscillations of two-dimensional panels with simply supported and clamped edge conditions. Rao and Rao<sup>27</sup> also employed the finite element displacement method to study the large amplitude supersonic flutter problems of two-dimensional panels with ends restrained elastically against rotation. In Refs. 25-27, the incremental stiffness matrices for the two-dimensional panels were derived by neglecting the in-plane strain due to  $\partial u/\partial x$  and by using the quasisteady aerodynamic theory. The two edges were restrained from in-plane displacements. Thus far, the finite element application to treat the large amplitude panel flutter problems has not been extended to the three-dimensional case, i.e., rectangular panels with finite aspect ratio.

In order to properly treat the large amplitude flutter problems of three-dimensional panels using the finite element approach, accurate and efficient formulations must first be chosen or developed for certain plate finite elements and be tested for a variety of the large amplitude free vibration and postbuckling problems of plates in the absence of aerodynamic pressure. The present writers<sup>28</sup> have extended the formulation of the 54 degree-of-freedom (DOF) triangular curved shell element developed by Dawe<sup>29</sup> for small deflection analysis to include the geometrically nonlinear terms for the case of flat plate. The bending portion of the linear formulation related to small transverse deflection is identical to that developed for the triangular plate bending element with 18 generalized coordinates by Cowper et al.<sup>30</sup> The formulation in Ref. 28 has been tested through its performance in a wide variety of geometrically nonlinear plate problems with high accuracies: large static deflection, postbuckling, large amplitude vibration with initial stresses, and linear vibration of a buckled plate. For this triangular finite element, each corner node has six degrees of freedom related to each of the three displacement components,  $u$ ,  $v$ , and  $w$ . The six degrees of freedom include the displacement com-

Received Aug. 25, 1982; revision received Jan. 4, 1983. Copyright © American Institute of Aeronautics and Astronautics, Inc., 1983. All rights reserved.

\*Graduate Student, School of Aeronautics and Astronautics.

†Professor and Head, School of Aeronautics and Astronautics. Associate Fellow AIAA.

ponent and its derivatives with respect to  $x$  and  $y$  up to the second order. The inclusion of the high-order in-plane displacement functions enables the element to more accurately and efficiently account for the coupling effect between the in-plane and transverse displacements.

In this study, the development in Ref. 28 is extended to investigate the limit cycle oscillation problems of two- and three-dimensional panels in supersonic flow. The effects of air-mass ratio, in-plane stresses, and various out-of-plane and in-plane boundary conditions are studied. The flutter boundaries for both the panels with static pressure differential and a panel buckled under in-plane stresses are obtained. The present results are compared with those obtained using alternative finite element and analytical approximate methods and discussions are provided.

### Nonlinear Finite Element Panel Flutter Equations

A thin elastic flat plate with thickness  $h$ , length  $L$ , width  $S$ , and mass density per unit volume  $\rho$  is shown in Fig. 1. One face of the plate is exposed to a supersonic airstream flowing along the  $x$  direction with air density  $\rho_a$ , flow velocity  $V_a$ , Mach number  $M$ , and aerodynamic pressure  $p_a$ . The plate is also subjected to biaxial in-plane stress resultant per unit length  $N_x$  and  $N_y$ , respectively. In addition to the aerodynamic pressure, the plate is subjected to a static uniform pressure differential,  $P_s$ .

The equation of motion for a thin elastic finite element plate in the presence of geometrical nonlinearity may be derived by means of Hamilton's principle,

$$\delta \int_{t_1}^{t_2} (T - U - V) dt + \int_{t_1}^{t_2} \delta W dt = 0 \quad (1)$$

where  $T$  is the kinetic energy,  $U$  the strain energy,  $V$  the potential energy of the applied conservative loads, and  $W$  the work done by the applied unconservative loads. In this study, the conservative loads are the in-plane forces and static pressure differential and the nonconservative loads are the aerodynamic pressure induced by the plate motion.

The kinetic energy due to the transverse oscillation of the plate is

$$T = \frac{\rho h}{2} \iint \left( \frac{\partial w}{\partial t} \right)^2 dx dy \quad (2)$$

The strain energy due to large deflection is

$$U = U_1 + U_2 + U_3 + U_4 \quad (3)$$

where

$$U_1 = \frac{6D}{h^2} \iint \left\{ \left( \frac{\partial u}{\partial x} \right)^2 + 2\nu \left( \frac{\partial u}{\partial x} \right) \left( \frac{\partial v}{\partial y} \right) + \left( \frac{\partial v}{\partial y} \right)^2 + \frac{1-\nu}{2} \left( \frac{\partial u}{\partial y} + \frac{\partial v}{\partial x} \right)^2 \right\} dx dy \quad (4)$$

$$U_2 = \frac{D}{2} \iint \left\{ \left( \frac{\partial^2 w}{\partial x^2} \right)^2 + 2\nu \left( \frac{\partial^2 w}{\partial x^2} \right) \left( \frac{\partial^2 w}{\partial y^2} \right) + \left( \frac{\partial^2 w}{\partial y^2} \right)^2 + 2(1-\nu) \left( \frac{\partial^2 w}{\partial x \partial y} \right)^2 \right\} dx dy \quad (5)$$

$$U_3 = \frac{6D}{h^2} \iint \left\{ \left( \frac{\partial u}{\partial x} + \nu \frac{\partial v}{\partial y} \right) \left( \frac{\partial w}{\partial x} \right)^2 + \left( \frac{\partial v}{\partial y} + \nu \frac{\partial u}{\partial x} \right) \times \left( \frac{\partial w}{\partial y} \right)^2 + (1-\nu) \left( \frac{\partial u}{\partial y} + \frac{\partial v}{\partial x} \right) \left( \frac{\partial w}{\partial x} \right) \left( \frac{\partial w}{\partial y} \right) \right\} dx dy \quad (6)$$

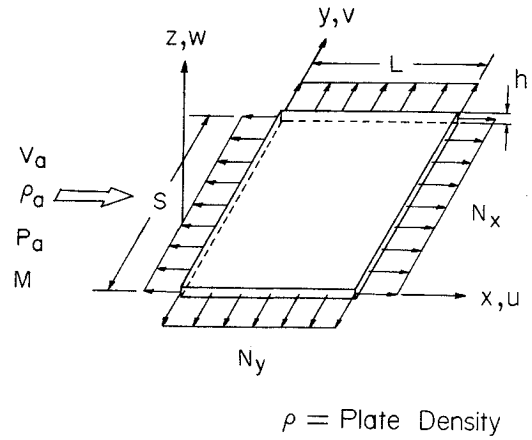


Fig. 1 Panel configuration.

$$U_4 = \frac{3D}{2h^2} \iint \left\{ \left( \frac{\partial w}{\partial x} \right)^2 + \left( \frac{\partial w}{\partial y} \right)^2 \right\} dx dy \quad (7)$$

and  $D = Eh^3/12(1-\nu^2)$  is the plate bending rigidity.

The potential energy due to the applied conservative loads is

$$V = \frac{1}{2} \iint \left\{ N_x \left( \frac{\partial w}{\partial x} \right)^2 + N_y \left( \frac{\partial w}{\partial y} \right)^2 + 2N_{xy} \left( \frac{\partial w}{\partial x} \right) \left( \frac{\partial w}{\partial y} \right) \right\} dx dy + \iint P_s w dx dy \quad (8)$$

The work done by the applied unconservative loads is

$$W = \iint p_a w dx dy \quad (9)$$

In the above expressions, the integration is performed over the area of the finite element. The aerodynamic pressure loading will be assumed to be that of quasisteady, supersonic theory:

$$p_a(x, y, t) = \frac{-\rho_a V_a^2}{\sqrt{M^2 - 1}} \left( \frac{\partial w}{\partial x} + \frac{M^2 - 2}{M^2 - 1} \frac{1}{V_a} \frac{\partial w}{\partial t} \right) \quad (10)$$

The finite element to be formulated for the present flutter analysis is based on the 54 DOF triangular curved element developed by Dawe<sup>29</sup> for linear shell analysis, which has been extended by the present writers<sup>28</sup> to include the geometrically nonlinear terms for the analysis of large deflection, post-buckling, and large amplitude vibration of plates. The displacement function for each of the three displacements  $u, v$ , and  $w$  is represented by a two-dimensional polynomial of complete quintic order of  $\xi$  and  $\eta$  minus the term  $\xi^4 \eta$ . The coordinate axis  $\xi$  coincides with edge 1-2 of the triangular element. The axis  $\eta$  passes through corner 3 and is perpendicular to the  $\xi$  axis. The term  $\xi^4 \eta$  is omitted to ensure that the slope normal to the edge  $\eta = 0$  is in the form of a cubic polynomial. Two further constraints are imposed to ensure that the slopes normal to the remaining two edges of the element are also in the form of cubic polynomials. The number of independent coefficients is thus reduced to 18 per displacement component. Each corner node then has 18 degrees of freedom, i.e., the three displacements  $u, v$ , and  $w$  and their complete first- and second-order derivatives with respect to the global coordinates  $x$  and  $y$ , respectively. It should be noted that the portion of the present stiffness matrix related to small transverse displacement  $w$  was first developed by Cowper et al.<sup>30</sup> based on Kirchhoff's plate

theory. The differences between the elements of Refs. 29 and 30 are that the former element possesses double curvatures and three quintic-order displacement functions  $u$ ,  $v$ , and  $w$ , respectively, whereas the latter element is flat and possesses only a quintic-order transverse displacement function  $w$ . The differences between the elements of Refs. 28 and 29 are that the element of Ref. 28 is flat but includes the incremental stiffness matrices which account for the effect of geometrically nonlinear large displacements. Furthermore, the in-plane displacements  $u$  and  $v$  and the out-of-plane displacement  $w$  in Ref. 28 are coupled. Thus, the important and more realistic boundary conditions related to in-plane displacements  $u$  and  $v$  can also be treated.

Substituting the displacement function for the plate finite element into Eqs. (2-10) and then minimizing the Hamiltonian in Eq. (1) with respect to each of the 54 nodal degrees of freedom yield the matrix equations of motion,

$$[m]\{\ddot{q}\} + \frac{\rho_a V_a (M^2 - 2)}{(M^2 - 1)^{3/2}} [d]\{\dot{q}\} + \frac{\rho_a V_a^2}{(M^2 - 1)^{1/2}} [a]\{q\} + \left[ [k] + [\sigma] + \frac{1}{2} [n_1] + \frac{1}{3} [n_2] \right] \{q\} = \{p\} \quad (11)$$

where  $[m]$ ,  $[d]$ , and  $[a]$  are the consistent mass, aerodynamic damping, and aerodynamic matrices, respectively, for the element;  $[k]$ ,  $[\sigma]$ ,  $[n_1]$ , and  $[n_2]$  are the linear stiffness, initial stress, first-order, and second-order incremental stiffness matrices, respectively; the vector  $\{q\}$  contains the nodal degrees of freedom; and the vector  $\{p\}$  contains the consistent load. The explicit expressions for the matrices  $[k]$ ,  $[n_1]$ ,  $[n_2]$ , and  $[m]$  were given in Ref. 28. The explicit expressions for matrices  $[a]$  and  $[\sigma]$  were given in Refs. 13 and 31, respectively. If the mass density and the thickness are constant throughout the plate and if the rotatory inertia is neglected,

$$[d] = I/\rho h [m] \quad (12)$$

By assembling the finite elements for the entire plate system and applying the kinematic boundary conditions, the equations of motion can be partitioned and written in the following form using capital letters,

$$\begin{aligned} & \left[ \begin{array}{c|c} 0 & 0 \\ \hline 0 & M \end{array} \right] \left\{ \begin{array}{c} \ddot{Q}_m \\ \ddot{Q}_f \end{array} \right\} + \bar{g} \left[ \begin{array}{c|c} 0 & 0 \\ \hline 0 & D \end{array} \right] \left\{ \begin{array}{c} \dot{Q}_m \\ \dot{Q}_f \end{array} \right\} \\ & + \bar{\lambda} \left[ \begin{array}{c|c} 0 & 0 \\ \hline 0 & A \end{array} \right] \left\{ \begin{array}{c} Q_m \\ Q_f \end{array} \right\} + \left[ \begin{array}{c|c} K_{mm} & 0 \\ \hline 0 & K_{ff} \end{array} \right] \left\{ \begin{array}{c} Q_m \\ Q_f \end{array} \right\} \\ & + \left[ \begin{array}{c|c} 0 & 0 \\ \hline 0 & \Sigma \end{array} \right] + \frac{1}{2} \left[ \begin{array}{c|c} 0 & N_{1mf} \\ \hline N_{1fm} & N_{1ff} \end{array} \right] \\ & + \frac{1}{3} \left[ \begin{array}{c|c} 0 & 0 \\ \hline 0 & N_{2ff} \end{array} \right] \left\{ \begin{array}{c} Q_m \\ Q_f \end{array} \right\} = \left\{ \begin{array}{c} 0 \\ P_f \end{array} \right\} \quad (13) \end{aligned}$$

where the subscripts  $m$  and  $f$  indicate membrane and flexure, respectively. In Eq. (13),  $\bar{g}$  and  $\bar{\lambda}$  are the aerodynamic damping and pressure parameters, respectively, and are

defined as

$$\bar{\lambda} = \rho_a V_a^2 / (M^2 - 1)^{1/2} \quad (14)$$

$$\bar{g} = \rho_a V_a (M^2 - 2) / (M^2 - 1)^{3/2} \quad (15)$$

It has been shown by flutter experiments that the flutter motion of the plates in limit cycle oscillation is approximately sinusoidal. The time function for the limit oscillation has thus been represented by using a sine or cosine function and the higher harmonic terms have been neglected.<sup>8,9</sup> Based on such assumptions, the equations of motion, Eq. (13), can be linearized and reduced to the following form:

$$[M]\{\ddot{Q}_f\} + \bar{g}[D]\{\dot{Q}_f\} + \bar{\lambda}[A]\{Q_f\} + \left[ [K_{ff}] + [\Sigma] + \frac{1}{4} [\bar{K}] \right] \{Q_f\} = \{P_f\} \quad (16)$$

where

$$[\bar{K}] = \frac{1}{2} [N_{1ff}] + \frac{1}{3} [N_{2ff}] - \frac{1}{4} [N_{1fm}] [K_{mm}]^{-1} [N_{1mf}] \quad (17)$$

### Solution Procedure

In order to solve Eq. (16), the displacement vector is assumed as an exponential function of time,

$$\{Q_f\} = \{\bar{Q}_f\} e^{\alpha t} \quad (18)$$

where  $\alpha$  is a complex number,  $\alpha = \beta + i\omega$ . When there is no static pressure acting on the plate, the load vector  $\{P_f\}$  vanishes and the equation of motion becomes

$$\left[ -\bar{\kappa}[M] + \bar{\lambda}[A] + [K_{ff}] + [\Sigma] + \frac{1}{4} [\bar{K}] \right] \{\bar{Q}_f\} = \{0\} \quad (19)$$

where  $\bar{\kappa} = -\alpha^2 - \bar{g}\alpha/\rho h$ .

To solve the nonlinear eigenvalue equation (19), an iterative procedure is used.<sup>25-28</sup> For a given set of aerodynamic pressure  $\bar{\lambda}$ , in-plane forces, mode number, and maximum amplitude, the iteration starts from a corresponding initial mode shape obtained from linear flutter analysis, with amplitude scaled up by a factor. Based on this initial mode shape, the nonlinear stiffness matrix  $[\bar{K}]$  is formed and an eigenvalue and its corresponding vector are found. This eigenvector is then scaled up again and the iteration continues until the convergence criteria  $\|\epsilon\|$  for  $\bar{\kappa}$  is achieved,

$$\|\epsilon\| = \left| \frac{\Delta \bar{\kappa}_i}{\bar{\kappa}_i} \right| \leq 10^{-3} \quad (20)$$

where  $\Delta \bar{\kappa}_i$  is the change in eigenvalue during the  $i$ th iterative cycle.

As indicated by the previous investigators,<sup>25-27</sup> when  $\bar{\lambda} = 0$  the problem is reduced to that of finding the in-vacuo frequencies for large amplitude free vibration of plates. As the dynamic pressure  $\bar{\lambda}$  is increased from zero, two of these eigenvalues will usually approach each other and coalesce to  $\bar{\kappa}_{cr}$  at  $\bar{\lambda} = \bar{\lambda}_{cr}$  and become complex conjugate pairs

$$\bar{\kappa} = \bar{\kappa}_R \pm i\bar{\kappa}_I \quad (21)$$

for  $\bar{\lambda} > \bar{\lambda}_{cr}$ . Here  $\bar{\lambda}_{cr}$  is considered to be that value of  $\bar{\lambda}$  at which first coalescence occurs for a specific amplitude of the limit cycle oscillation.

In the absence of aerodynamic damping,  $\bar{g} = 0$ , the flutter dynamic pressure for limit cycle oscillation is equal to the value of  $\bar{\lambda}_{cr}$  and  $\alpha = i\sqrt{\bar{\kappa}_R}$ . In the presence of  $\bar{g}$ , Eq. (15) may

be expressed as

$$\bar{g} = \left(\frac{\mu}{M}\right)^{1/2} \left(\frac{\lambda \rho h}{L}\right)^{1/2} \quad (22)$$

where  $\mu = \rho_a L / \rho h$  is the air-panel mass ratio and for  $M \gg 1$

$$\left(\frac{M^2 - 2}{M^2 - 1}\right)^2 \left(\frac{\mu}{\sqrt{M^2 - 1}}\right) \approx \frac{\mu}{M} \quad (23)$$

When  $\bar{\lambda} > \bar{\lambda}_{cr}$ , the eigenvalue solution for  $\bar{\kappa}$  in Eq. (19) becomes complex,

$$\bar{\kappa} = -\alpha^2 - \bar{g}\alpha / \rho h = \bar{\kappa}_R - i\kappa_I \quad (24)$$

The limit cycle oscillation is reached when

$$\bar{g} / \rho h = \bar{\kappa}_I / \sqrt{\bar{\kappa}_R} \quad (25)$$

For

$$\bar{g} / \rho h < \bar{\kappa}_I / \sqrt{\bar{\kappa}_R} \quad (26)$$

$\beta$  becomes positive, the amplitude will increase with time.

For flutter analysis of plates subjected to static pressure differential, the equations of motion can be obtained from Eq. (13) by neglecting the initial stress matrix  $[\Sigma]$ . The static equilibrium state is solved using the Newton-Raphson approach where the time-dependent terms are neglected first. After the static equilibrium state is obtained, the incremental stiffness matrices  $[N_1]$  and  $[N_2]$  can then be formulated. Linear flutter analysis for the plate with small amplitude oscillation can then be performed with reference to this large displacement equilibrium state. In the absence of  $[\Sigma]$ , Eq. (13) may be simplified by writing all of the in-plane degrees of freedom in terms of the flexural degrees of freedom first and then eliminating them through matrix partition and substitution. Thus, only the flexural degrees of freedom remain,

$$[M]\{\ddot{Q}_f\} + \bar{g}[D]\{\dot{Q}_f\} + [\bar{\lambda}[A] + [K_{ff}] + [\bar{K}']]\{Q_f\} = \{0\} \quad (27)$$

where

$$[\bar{K}'] = [N_{1ff}] + [N_{2ff}] - [N_{1fm}][K_{mm}]^{-1}[N_{1mf}] \quad (28)$$

By assuming the displacement vector  $\{Q_f\}$  as the exponential function of time as shown in Eq. (18), Eq. (27) can then be expressed as

$$[-\bar{\kappa}[M] + \bar{\lambda}[A] + [K_{ff}] + [\bar{K}']]\{\bar{Q}_f\} = \{0\} \quad (29)$$

To find the linear flutter boundary for a plate subjected to static pressure differential is to solve the simplified eigenvalue equation (29) by gradually increasing the dynamic pressure  $\bar{\lambda}$ . When the aerodynamic damping  $\bar{g} = 0$ , the coalescence of two of these eigenvalues gives the flutter solution. When  $\bar{g} > 0$ , the flutter solution is obtained when  $\bar{g} = \rho h \bar{\kappa}_I / \sqrt{\bar{\kappa}_R}$ , as defined in Eq. (25).

For convenience of comparison of the present results with alternative existing solutions, the nondimensional aerodynamic pressure  $\lambda$ , aerodynamic damping  $g_a$ , and the eigenvalue  $\kappa$  are defined consistently with those commonly defined as

$$\lambda = \bar{\lambda} L^3 / D \quad (30)$$

$$g_a = \left(\frac{\mu}{M}\right)^{1/2} = \left(\frac{\bar{g}}{\rho h}\right) \left(\frac{\rho h L^4}{D}\right)^{1/2} \quad (31)$$

$$\kappa = \kappa_R \pm i\kappa_I = \bar{\kappa} \left(\frac{\rho h L^4}{D}\right) \quad (32)$$

## Results and Discussion

The incremental stiffness formulation for the present 54 DOF triangular plate element has been evaluated in Ref. 28 by analyzing a variety of plate problems including large deflection, postbuckling, and large amplitude vibration. The formulation for this element has been extended to include the effect of supersonic aerodynamic pressure. Before applying this formulation to solve the nonlinear panel flutter problems, it is necessary to conduct a linear panel flutter analysis to evaluate the aerodynamic portion of the formulation and to determine suitable mesh sizes.

### Linear Flutter Analysis

For linear flutter analysis of plates only the flexural displacement need be considered. Due to the symmetrical nature of the aerodynamic forces about the centerline of the plate along the flow direction, only half of each plate was used. The eigenvalue coalescence results obtained by using four different kinds of finite element meshes for a simply supported and a clamped square plate are shown in Table 1. This table also shows two alternative finite element solutions<sup>13,17</sup> and the analytical solutions.<sup>31</sup> It is seen that the present finite element solutions are quite accurate even for relatively coarse meshes.

In the following nonlinear flutter analysis, the single-layer 8-element mesh shown in Table 1 was used. This mesh is seen to give sufficiently good accuracy in the linear flutter analysis. This mesh had also been found to give results with sufficiently good accuracy when tested for all the nonlinear plate examples of Ref. 28.

### Limit Cycle Oscillations

A two-dimensional, simply supported panel was first considered. A strip was modeled using a  $5 \times 2$  grid point mesh or eight triangular elements. The results for eigenvalue  $\kappa_n$  vs dynamic pressure  $\lambda$  are plotted in Fig. 2 for two amplitude ratios,  $w/h = 0$  and  $w/h = 0.6$ , respectively.

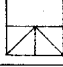
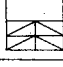
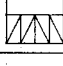

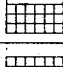
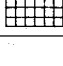
For  $w/h = 0$ , the two sets of eigenvalues coalesce at  $\lambda_{cr} = 343.35$ , which is the critical dynamic pressure for linear flutter with no aerodynamic damping. When  $\lambda > 343.35$ , the eigenvalue becomes complex and the flutter can occur at a value higher than  $\lambda_{cr}$  if some aerodynamic damping is present. This  $\lambda$  value is obtained by an iterative procedure when the value of aerodynamic damping  $g_a$  defined as  $\sqrt{\lambda\mu}/M$ , and the value of  $\kappa_I / \sqrt{\kappa_R}$  as obtained in Fig. 2 are equal.

For  $w/h = 0.6$ , the two sets of eigenvalues coalesce at  $\lambda = 438.6$  and become complex at  $\lambda > 438.6$ . For the case of negligible aerodynamic damping,  $g_a \rightarrow 0$ , the limit cycle oscillation occurs at  $\lambda = 438.6$ . If some aerodynamic damping is present, the limit cycle oscillation occurs at a higher  $\lambda$  value. This value is found by an iterative procedure as  $g_a = \kappa_I / \sqrt{\kappa_R}$ .

A complete parallel set of results obtained by Mei<sup>26</sup> and a coalesced  $\lambda$  value for  $w/h = 0.6$  obtained by Rao and Rao<sup>27</sup> are also shown in Fig. 2 for comparison. In both Refs. 26 and 27, eight beam elements were used by neglecting the axial strain term  $1/2 u / 1/2 x$ . In Ref. 27, the strain energy was further linearized.

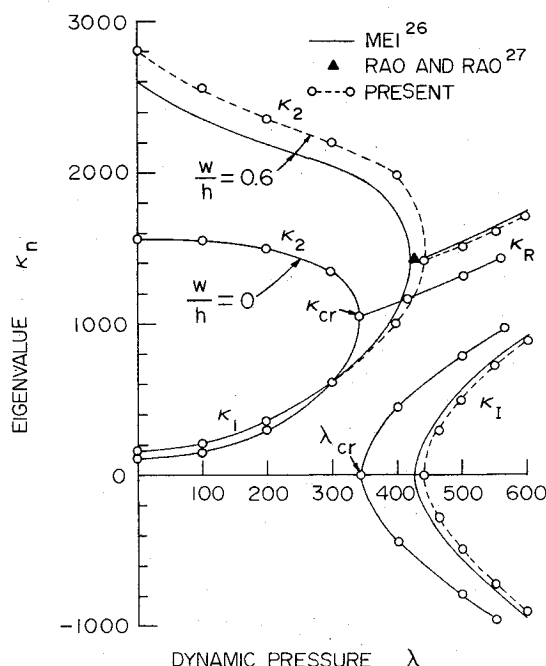
The results for the amplitude of limit cycle oscillation ( $w/h$  at  $x = 0.75L$ ) vs dynamic pressure  $\lambda$  for the two-dimensional simply supported panel are shown in Fig. 3. Two values of mass ratio ( $\mu/M = 0.01$  and  $0.1$ ) and three values of axial compressive force ( $R_x = N_x L^2 / D = 0, -\pi^2$ , and  $-2\pi^2$ ) were considered. For each assumed value of amplitude, mass ratio, and in-plane force, the dynamic pressure for limit cycle oscillation is obtained by iteration such that  $g_a = \sqrt{\lambda\mu}/M = \kappa_I / \sqrt{\kappa_R}$ . The results obtained by Dowell<sup>3</sup> using a time-integration

**Table 1** Eigenvalue coalescence results for linear flutter analysis of a simply-supported and a clamped square plate.

FINITE ELEMENT	MESH FOR HALF OF THE PLATE	SIMPLY-SUPPORTED			CLAMPED		
		D.O.F.'S	DYNAMIC PRESSURE $\lambda_{cr}$	EIGENVALUE $K_{cr}$	D.O.F.'S	DYNAMIC PRESSURE $\lambda_{cr}$	EIGENVALUE $K_{cr}$
PRESENT 18 D.O.F. TRIANGULAR ELEMENT		13	514.060	1848.76	7	914.183	4514.54
		25	511.436	1838.48	15	844.483	4198.52
		27	513.366	1847.26	20	879.264	4380.53
		51	512.334	1846.55	37	852.729	4294.07
16 D.O.F. RECTANGULAR ELEMENT <sup>13</sup>		72	511.786	1843.29	50	850.418	4282.03
16 D.O.F. QUADRILATERAL ELEMENT <sup>17</sup>		179*	512.200	1844.00	135*	853.400	4292.00
EXACT SOLUTION <sup>31</sup>			512.651	1848.21		876.800 <sup>†</sup>	4077.00 <sup>†</sup>

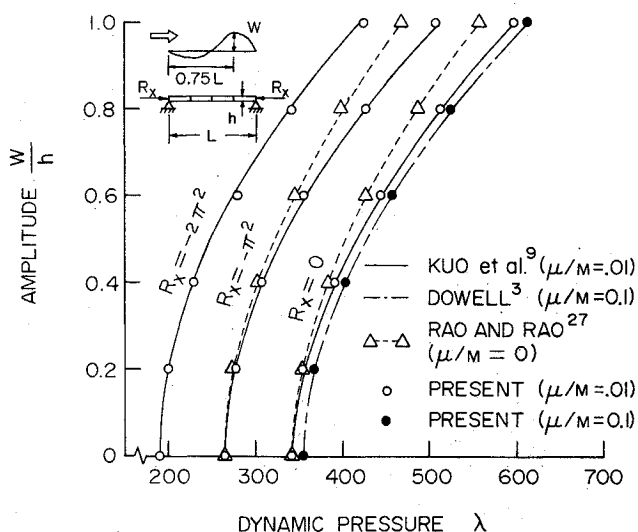
\* MESH FOR FULL PLATE

† APPROXIMATE SOLUTION

**Fig. 2** Eigenvalues vs dynamic pressure for the two-dimensional simply supported panel.

method, by Kuo et al.<sup>9</sup> using perturbation and harmonic balance methods, and Rao and Rao<sup>27</sup> using eight beam elements are also shown in Fig. 3 for comparison. The present results are in excellent agreement with those in Refs. 3 and 9. It is noted that the present results for  $\mu/M=0$  and  $\mu/M=0.01$  are found to be very close so that only the latter results are shown.

The results for the distribution of the nondimensional total stress in the upper and lower extreme fibers along the chordwise direction are shown in Fig. 4 for  $\mu/M=0.01$  and for  $\lambda=400$  and 500, respectively. Both 8 and 16 element meshes were used and the two sets of results are very close. The upper

**Fig. 3** Limit cycle amplitude vs dynamic pressure for the two-dimensional simply supported panel.

and lower extreme fiber stresses are symmetric about a nonzero mean value, which is the in-plane tensile stress due to large deflection. The results obtained by Dowell<sup>3</sup> using a time-integration method based on six modes are also shown in Fig. 4 for comparison. The agreement is very good.

A two-dimensional clamped panel was considered next. The results for the amplitude of limit cycle oscillation ( $w/h$  at  $x=0.75L$ ) vs dynamic pressure  $\lambda$  using eight triangular plate elements are shown in Fig. 5. Two values of mass ratio ( $\mu/M=0$  and 0.1) and three values of axial compressive forces ( $R_x=0$ ,  $-\pi^2$ , and  $-2\pi^2$ ) were considered. The results obtained by Rao and Rao<sup>27</sup> for  $\mu/M=0$  using eight beam elements are also shown for comparison. The agreement is close.

The results for the additional boundary condition that the two edges are free to move in the plane of the panel are also

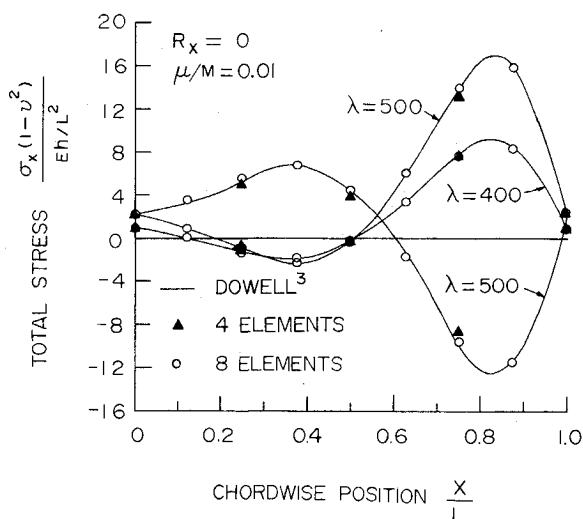


Fig. 4 Chordwise stress distribution along panel for the two-dimensional simply supported panel.

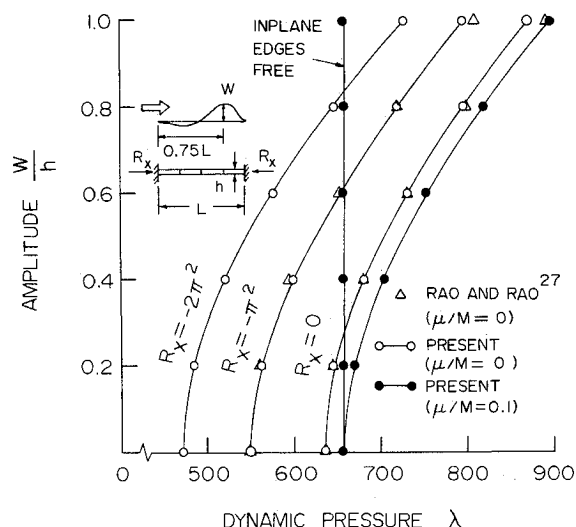


Fig. 5 Limit cycle amplitude vs dynamic pressure for the two-dimensional clamped panel with in-plane edges fixed.

shown in Fig. 5. Similar results were obtained by Dowell.<sup>3</sup> It is of interest to see that due to the absence of in-plane stretching, the dynamic pressure is independent of the amplitude and is equal to the critical value for linear flutter. Such conclusion has also been found for the two-dimensional simply supported panel, but the results are not shown in Fig. 3.

The third case considered was a simply supported square plate. The results for the amplitude of limit cycle oscillation ( $w/h$  at  $x=0.75L$  on the centerline) vs dynamic pressure  $\lambda$  using eight triangular elements to model half of the plate are shown in Fig. 6. Two values of mass ratio ( $\mu/M=0.01$  and  $0.1$ ) and two values of biaxial compressive forces ( $R_x=R_y=N_xL^2/D=0$  and  $-2\pi^2$ ) were considered. The results by Dowell<sup>3</sup> using a time-integration method based on six modes are also shown in Fig. 6 for comparison. The agreement is excellent. The boundary condition for edges free to move in the plane of the panel was also considered with results shown in Fig. 6. The amplitudes of limit cycle oscillation are considerably larger than those for the panel with in-plane edges fixed.

The fourth case considered was a clamped square plate and the results are shown in Fig. 7. The results by Ventres and Dowell<sup>5</sup> and by Kuo et al.<sup>9</sup> are also shown in Fig. 7 for comparison. The agreement is excellent.

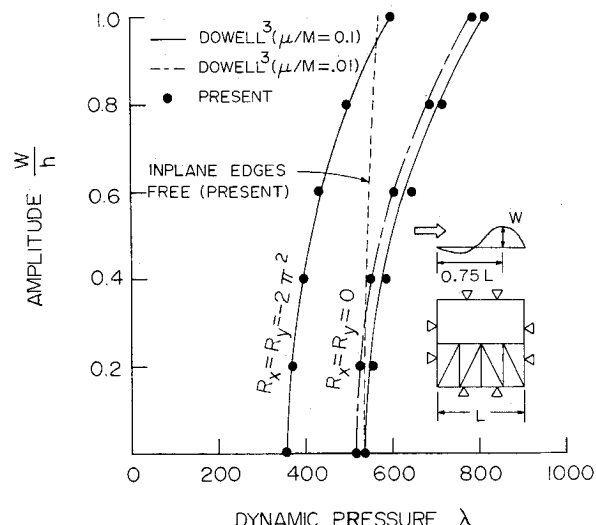


Fig. 6 Limit cycle amplitude vs dynamic pressure for the simply supported square plate with in-plane edges fixed.

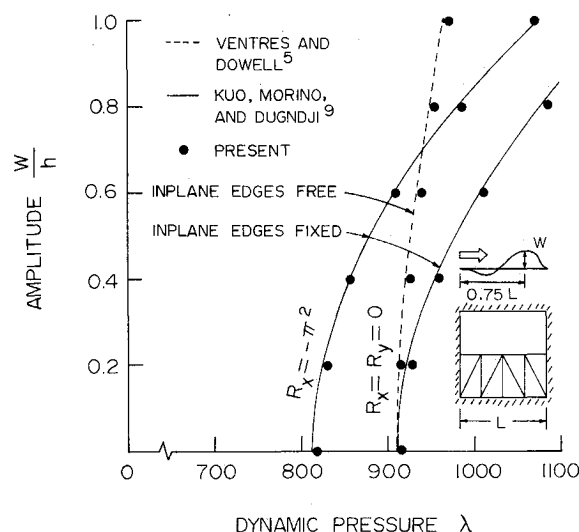


Fig. 7 Limit cycle amplitude vs dynamic pressure for the clamped square plate ( $\mu/M=0.1$ ).

#### Flutter of Panels Under Static Pressure Differential

A simply supported and a clamped two-dimensional plate were first considered. The plates were subjected to a static pressure differential  $P_s$  and a dynamic pressure  $\lambda$ . The results for the steady mean amplitude ( $W_s/h$  at  $x=0.75L$ ) vs static pressure differential parameter  $P_sL^4/Dh$  for various values of  $\lambda$  are given in Fig. 8 for both plates. The results for the simply supported plate are practically in total agreement with those obtained by Dowell.<sup>3</sup>

Based on a state of mean steady equilibrium under a pressure differential  $P_s$ , the dynamic pressure corresponding to the flutter condition can be found for a certain value of mass ratio  $\mu/M$ . This is done by an iterative procedure to search for the  $\lambda$  value such that the aerodynamic damping parameter  $\sqrt{\mu/M}$  and the value of  $\kappa_I/\sqrt{\kappa_R}$  found from the complex eigenvalue are equal. The flutter boundaries plotted as  $\lambda$  vs  $P_s$  for  $\mu/M=0.1$  are shown in Fig. 9 for both plates. The results for the simply supported plate obtained by Dowell<sup>3</sup> are also shown for comparison. The agreement is excellent.

A simply supported and a clamped square plate were then considered. The results for the steady mean amplitude ( $W_s/h$  at  $0.75L$  on the centerline) vs static pressure differential  $P_s$  for various  $\lambda$  values are shown in Fig. 10 and the flutter bound-

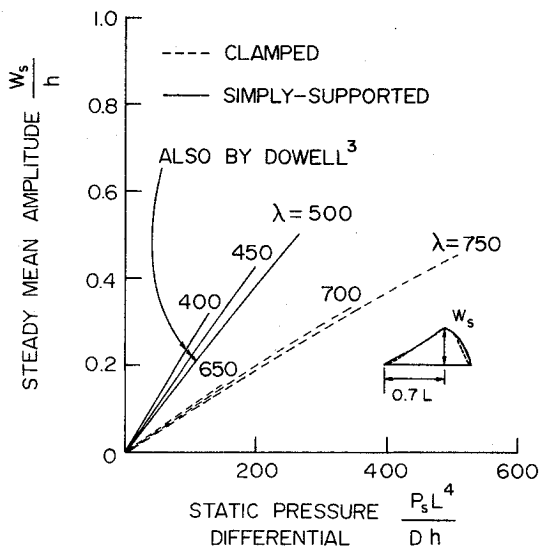


Fig. 8 Steady mean amplitude vs static pressure differential for the two-dimensional panels.

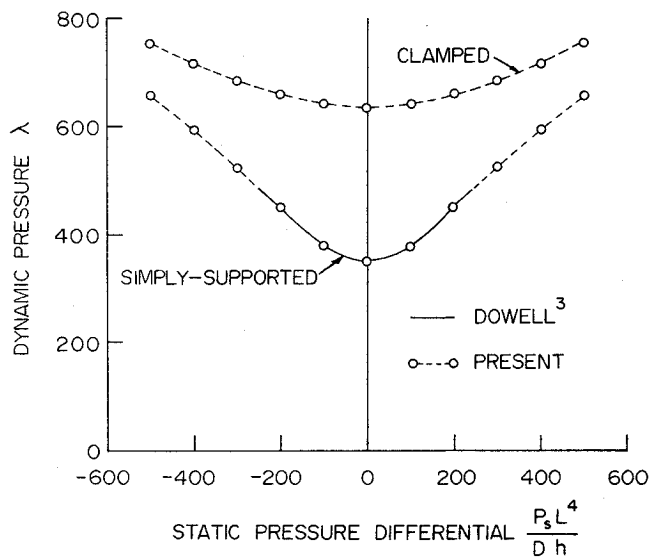


Fig. 9 Flutter dynamic pressure vs static pressure differential for the two-dimensional panels ( $\mu/M=0.01$ ).

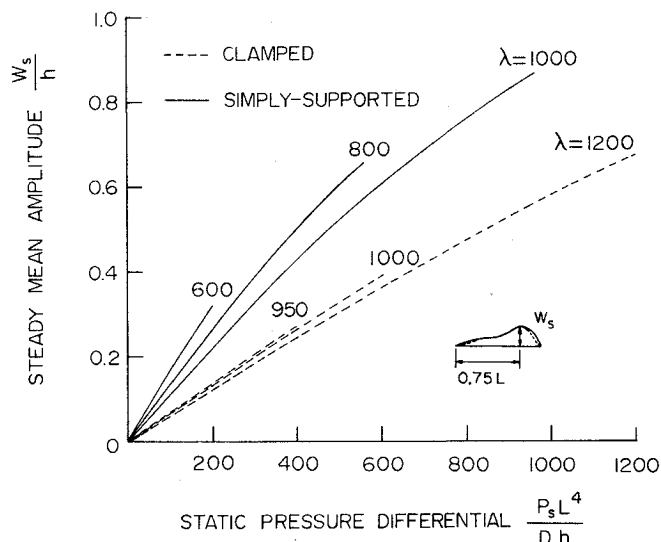


Fig. 10 Steady mean amplitude vs static pressure differential for the square plates.

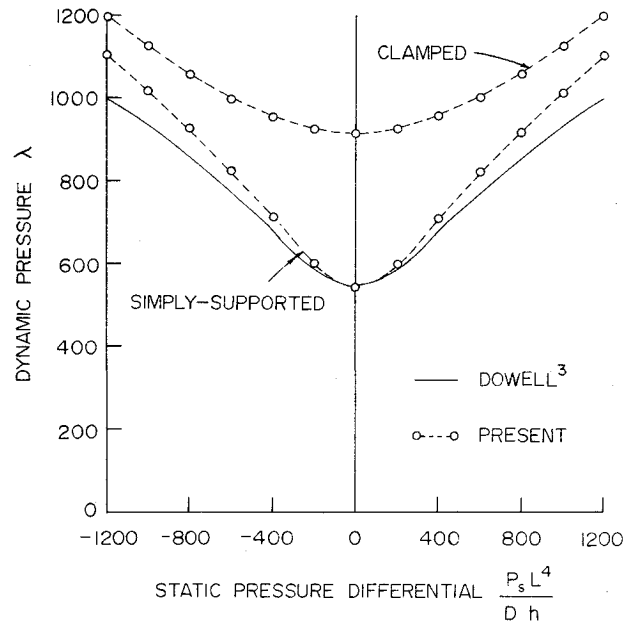


Fig. 11 Flutter dynamic pressure vs static pressure differential for the square plates ( $\mu/M=0.1$ ).

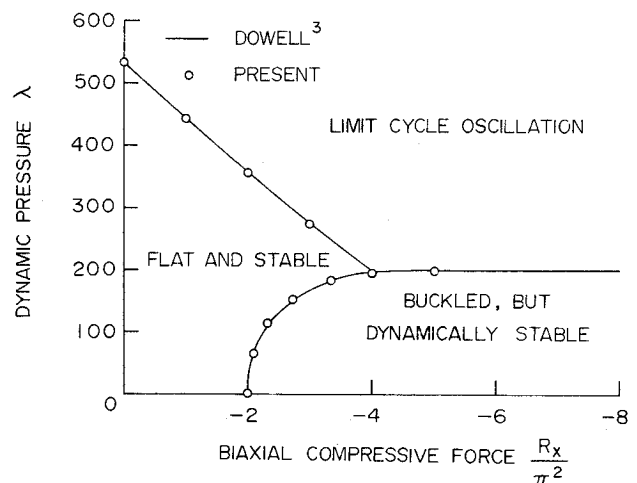


Fig. 12 Stability regions for the simply supported square plate.

aries plotted as  $\lambda$  vs  $P_s$  for  $\mu/M=0.1$  are shown in Fig. 11 for both plates. The results for the simply supported case by Dowell<sup>3</sup> are also shown for comparison. The discrepancy becomes larger as  $P_s$  increases. A maximum discrepancy of 10% is observed at  $P_s L^4 / D h = 1200$ .

#### Flutter of Buckled Panel

The effect of in-plane loading on the flutter boundaries for a simply supported square panel was studied. The results plotted as dynamic pressure  $\lambda$  vs biaxial in-plane compression  $R_x = R_y$  for  $\mu/M=0.1$  are shown in Fig. 12.

For the linear flutter boundary, the biaxial in-plane compression  $R_x$  has a destabilizing effect such that the  $\lambda$  value decreases as the compression increases. Below this boundary, the panel remains flat and stable, whereas above this boundary the plate undergoes a limit cycle oscillation.

For zero dynamic pressure, the plate buckles at  $R_x = -2\pi^2$ , the Euler buckling load. Due to the stabilizing effect of the dynamic pressure, the critical buckling value of  $R_x$  becomes higher for a higher  $\lambda$  value. Thus the  $\lambda$  vs  $R_x$  plot forms a boundary between the stable unbuckled region and the buckled but dynamically stable region. This boundary intersects the linear flutter boundary and after that a third boundary is formed.

Below this third boundary, the panel is buckled in a nonlinear, equilibrium, and dynamically stable state. Above this boundary the plate undergoes a limit cycle oscillation. A point on this boundary is obtained by an iterative process to solve for Eq. (19) and to search for the highest  $\lambda$  value corresponding to the zero frequency of the limit cycle oscillation. The parameters to be incremented in this iterative process include  $\lambda$ ,  $R_x$ , and amplitude.

### Concluding Remarks

Within the assumption of Kirchhoff's plate theory, a sophisticated 54 DOF triangular plate element originally developed by Dawe<sup>29</sup> for linear thin shell analysis was extended by the present writers<sup>28</sup> to include the geometric nonlinearities and has now been further extended to formulate and analyze the nonlinear supersonic panel flutter problems. The portion of the formulation related to the linear bending behavior is identical to that given in Ref. 30. Quasisteady aerodynamic theory has been used. The formulations and solution procedures have been evaluated by analyzing a variety of examples: 1) limit cycle oscillations; 2) flutter of panels under static pressure differential; and 3) flutter of a buckled panel. Alternative analytical and numerical solutions are available for most of the examples for comparison and all are in excellent agreement.

It is noted that the present examples contain panels with rectangular shape, thus the finite element solution based on Kirchhoff theory is smooth and overconformity at the vertices does not cause difficulties. The present development is not intended for the solution of plate problems that require the use of the Reissner-Mindlin<sup>33-35</sup> plate theory. For example, if a simply supported rhombic plate with acute angles of 30 deg subjected to uniform load is considered, a strong singularity will occur at the obtuse vertex when Kirchhoff theory is used. In that case, finite elements should be formulated based on the Reissner-Mindlin<sup>33-35</sup> plate theory. Discussion of this point can be found in, for example, Refs. 36-38. It has been shown in Refs. 37 and 38 that accurate and efficient solution for this example can be obtained with relatively coarse mesh and progressively higher  $p$ -values if the  $p$ -version finite elements based on the Reissner-Mindlin plate theory are used.

Thus far, the finite element application to treat large amplitude panel flutter problems has only been limited to the two-dimensional case, i.e., a wide beam or a strip. This development enables the finite element application to be widened to the three-dimensional case to include: rectangular panels with arbitrary aspect ratios and complex in-plane as well as out-of-plane boundary conditions; and panels with geometries for which the Kirchhoff plate theory can give satisfactory solutions in buckling loads and modes, flutter-related lower frequencies and modes, and postbuckling and large-amplitude vibration behaviors.

Some logical extensions may be worthy of mentioning: 1) panels with initial deflections; 2) use of linear potential aerodynamic theory for low supersonic Mach number; and 3) nonlinear aerodynamic loadings.

### References

- <sup>1</sup>Dowell, E.H., "Panel Flutter: A Review of the Aeroelastic Stability of Plates and Shells," *AIAA Journal*, Vol. 8, March 1970, pp. 385-399.
- <sup>2</sup>Dowell, E.H., *Aeroelasticity of Plates and Shells*, Noordhoff International Publishing, Leyden, the Netherlands, 1975.
- <sup>3</sup>Dowell, E.H., "Nonlinear Oscillations of a Fluttering Plate," *AIAA Journal*, Vol. 4, July 1966, pp. 1267-1275.
- <sup>4</sup>Dowell, E.H., "Nonlinear Oscillations of a Fluttering Plate II," *AIAA Journal*, Vol. 5, Oct. 1967, pp. 1856-1862.
- <sup>5</sup>Ventres, C.S. and Dowell, E.H., "Comparison of Theory and Experiment for Nonlinear Flutter of Loaded Plates," *AIAA Journal*, Vol. 8, Nov. 1970, pp. 2022-2030.

- <sup>6</sup>Kobayashi, S., "Flutter of Simply-Supported Rectangular Panels in a Supersonic Flow—Two-Dimensional Panel Flutter, I—Simply-Supported Panel, II—Clamped Panel," *Transactions of Japan Society of Aeronautical and Space Sciences*, Vol. 5, 1962, pp. 79-118.
- <sup>7</sup>Bolotin, V.V., *Nonconservative Problems of the Theory of Elastic Stability*, MacMillan Co., New York, 1963, pp. 274-312.
- <sup>8</sup>Eastep, F.E. and McIntosh, S.C., Jr., "Analysis of Nonlinear Panel Flutter and Response under Random Excitation or Nonlinear Aerodynamic Loading," *AIAA Journal*, Vol. 9, March 1971, pp. 411-418.
- <sup>9</sup>Kuo, C.C., Morino, L., and Dugundji, J., "Perturbation and Harmonic Balance Methods for Nonlinear Panel Flutter," *AIAA Journal*, Vol. 10, Nov. 1972, pp. 1479-1484.
- <sup>10</sup>Morino, L., "A Perturbation Method for Treating Nonlinear Panel Flutter Problems," *AIAA Journal*, Vol. 7, March 1969, pp. 405-411.
- <sup>11</sup>Smith, L. and Morino, L., "Stability Analysis of Nonlinear Differential Autonomous Systems with Applications to Flutter," *AIAA Journal*, Vol. 14, March 1976, pp. 333-341.
- <sup>12</sup>Olson, M.D., "Finite Elements Applied to Panel Flutter," *AIAA Journal*, Vol. 5, Dec. 1967, pp. 2267-2270.
- <sup>13</sup>Olson, M.D., "Some Flutter Solutions Using Finite Elements," *AIAA Journal*, Vol. 8, April 1970, pp. 747-752.
- <sup>14</sup>Appa, K. and Somashekar, B.R., "Application of Matrix Displacement Methods in the Study of Panel Flutter," *AIAA Journal*, Vol. 7, Jan. 1969, pp. 50-53.
- <sup>15</sup>Appa, K. and Somashekar, B.R., "Flutter of Skew Panels by the Matrix Displacement Approach," *The Aeronautical Journal of the Royal Aeronautical Society*, Vol. 74, Aug. 1970, pp. 672-675.
- <sup>16</sup>Appa, K., Somashekar, B.R., and Shah, C.G., "Discrete Element Approach to Flutter of Skew Panels with In-Plane Forces under Yawed Supersonic Flow," *AIAA Journal*, Vol. 8, Nov. 1970, pp. 2017-2022.
- <sup>17</sup>Sander, G., Bon, C., and Geradin, M., "Finite Element Analysis of Supersonic Panel Flutter," *International Journal for Numerical Methods in Engineering*, Vol. 7, 1973, pp. 379-394.
- <sup>18</sup>Rosettos, J.N. and Tong, P., "Finite Element Analysis of Vibration and Flutter of Cantilever Anisotropic Plates," *Journal of Applied Mechanics*, ASME Paper 74-WA/APM-15, 1974.
- <sup>19</sup>Bismarck-Nasr, M.N., "Finite Element Method Applied to the Supersonic Flutter of Circular Cylindrical Shells," *International Journal for Numerical Methods in Engineering*, Vol. 10, 1976, pp. 423-435.
- <sup>20</sup>Bismarck-Nasr, M.N., "Finite Element Method Applied to the Flutter of Two Parallel Elastically Coupled Flat Plates," *International Journal for Numerical Methods in Engineering*, Vol. 11, 1977, pp. 1188-1193.
- <sup>21</sup>Bismarck-Nasr, M.N. and Costa Savio, H.R., "Finite-Element Solution of the Supersonic Flutter of Conical Shells," *AIAA Journal*, Vol. 17, Oct. 1979, pp. 1148-1150.
- <sup>22</sup>Yang, T.Y., "Flutter of Flat Finite Element Panels in a Supersonic Potential Flow," *AIAA Journal*, Vol. 13, Nov. 1975, pp. 1502-1507.
- <sup>23</sup>Yang, T.Y. and Sung, S.H., "Finite-Element Panel Flutter in Three-Dimensional Supersonic Unsteady Potential Flow," *AIAA Journal*, Vol. 15, Dec. 1977, pp. 1677-1683.
- <sup>24</sup>Yang, T.Y. and Han, A.D., "Flutter of Thermally Buckled Finite Element Panels," *AIAA Journal*, Vol. 14, July 1976, pp. 975-977.
- <sup>25</sup>Mei, C. and Rogers, J.L. Jr., "Application of NASTRAN to Large Deflection Supersonic Flutter of Panels," NASA TMX-3428, 1976, pp. 67-97.
- <sup>26</sup>Mei, C., "A Finite-Element Approach for Nonlinear Panel Flutter," *AIAA Journal*, Vol. 15, Aug. 1977, pp. 1107-1110.



<sup>27</sup>Rao, K.S. and Rao, G.V., "Large Amplitude Supersonic Flutter of Panels with Ends Elastically Restrained Against Rotation," *Computers and Structures*, Vol. 11, 1980, pp. 197-201.

<sup>28</sup>Yang, T.Y. and Han, A.D., "Buckled Plate Vibrations and Large Amplitude Vibrations Using High-Order Triangular Elements," *AIAA Journal*, Vol. 21, May 1983, pp. 758-766.

<sup>29</sup>Dawe, D.J., "High-Order Triangular Finite Element for Shell Analysis," *International Journal of Solids and Structures*, Vol. 11, 1975, pp. 1097-1110.

<sup>30</sup>Cowper, G.R., Kosko, E., Lindberg, G.M., and Olson, M.D., "Static and Dynamic Applications of a High-Precision Triangular Plate Bending Element," *AIAA Journal*, Vol. 7, Oct. 1969, pp. 1957-1965.

<sup>31</sup>Tabarrok, B., Fenton, R.G., and Elsaie, A.M., "Application of a Refined Plate Bending Element to Buckling Problems," *Computers and Structures*, Vol. 4, 1974, pp. 1313-1321.

<sup>32</sup>Houbolt, J.C., "A Study of Several Aerothermoelastic Problems of Aircraft Structures in High Speed Flight," Ph.D. Thesis, No. 2760, Swiss Federal Institute of Technology, Zürich, Switzerland, 1958.

<sup>33</sup>Reissner, E., "The Effect of Transverse Shear Deformation on the Bending of Elastic Plates," *Journal of Applied Mechanics, Transactions of ASME*, Vol. 67, 1945, p. A-69.

<sup>34</sup>Reissner, E., "On Bending of Elastic Plates," *Quarterly of Applied Mathematics*, Vol. 5, 1947, pp. 55-68.

<sup>35</sup>Mindlin, R.D., "Influence of Rotatory Inertia and Shear on Flexural Motions of Isotropic, Elastic Plates," *Journal of Applied Mechanics*, Vol. 18, March 1951, pp. 31-38.

<sup>36</sup>Sander, G., "Application of the Dual Analysis Principle," *High Speed Computing of Elastic Structures, Proceedings of IUTAM Symposium*, Liege, Belgium, 1971, pp. 381-397.

<sup>37</sup>Szabo, B.A., Peano, A.G., Katz, I.N., and Rossow, M.P., "Advanced Finite Element Technology for Stress Analysis," Washington University, St. Louis, Mo., Rept. DOT-TST-76-71, 1976 (available through NTIS).

<sup>38</sup>Szabo, B.A., Basu, P.K., Dunavant, D.A., and Vasilopoulos, D., "Adaptive Finite Element Technology in Integrated Design and Analysis," Center for Computational Mechanics, Washington University, St. Louis, Mo., Rept. WU/CCM-81/1, Jan. 1981.

*From the AIAA Progress in Astronautics and Aeronautics Series . . .*

## **AEROTHERMODYNAMICS AND PLANETARY ENTRY—v. 77**

## **HEAT TRANSFER AND THERMAL CONTROL—v. 78**

*Edited by A. L. Crosbie, University of Missouri-Rolla*

The success of a flight into space rests on the success of the vehicle designer in maintaining a proper degree of thermal balance within the vehicle or thermal protection of the outer structure of the vehicle, as it encounters various remote and hostile environments. This thermal requirement applies to Earth-satellites, planetary spacecraft, entry vehicles, rocket nose cones, and in a very spectacular way, to the U.S. Space Shuttle, with its thermal protection system of tens of thousands of tiles fastened to its vulnerable external surfaces. Although the relevant technology might simply be called heat-transfer engineering, the advanced (and still advancing) character of the problems that have to be solved and the consequent need to resort to basic physics and basic fluid mechanics have prompted the practitioners of the field to call it thermophysics. It is the expectation of the editors and the authors of these volumes that the various sections therefore will be of interest to physicists, materials specialists, fluid dynamicists, and spacecraft engineers, as well as to heat-transfer engineers. Volume 77 is devoted to three main topics, Aerothermodynamics, Thermal Protection, and Planetary Entry. Volume 78 is devoted to Radiation Heat Transfer, Conduction Heat Transfer, Heat Pipes, and Thermal Control. In a broad sense, the former volume deals with the external situation between the spacecraft and its environment, whereas the latter volume deals mainly with the thermal processes occurring within the spacecraft that affect its temperature distribution. Both volumes bring forth new information and new theoretical treatments not previously published in book or journal literature.

*Volume 77—444 pp., 6 × 9, illus., \$30.00 Mem., \$45.00 List*

*Volume 78—538 pp., 6 × 9, illus., \$30.00 Mem., \$45.00 List*

TO ORDER WRITE: Publications Order Dept., AIAA, 1633 Broadway, New York, N.Y. 10019